Science
AAAS

Main Text for

Electrophotocatalytic perfluoroalkylation by LMCT excitation of Ag(II) perfluoroalkyl carboxylates

Brandon M. Campbell,[1] Jesse B. Gordon,[1] Elaine Reichert Raguram,[1] Miguel I. Gonzalez,[1] Kristopher G. Reynolds,[1] Matthew Nava[1,2] and Daniel G. Nocera[1,*]

Affiliations:

[1]Department of Chemistry and Chemical Biology, Harvard University; Cambridge, MA 02138, United States.

[2]Department of Chemistry and Biochemistry, University of California at Los Angeles, Los Angeles, CA 90095, United States.

*Corresponding author. Email: dnocera@fas.harvard.edu

Abstract: Molecular Ag(II) complexes are super-oxidizing photoredox catalysts capable of generating radicals from redox reticent substrates. Herein, we exploit the electrophilicity of Ag(II) centers in $[Ag(bpy)_2(TFA)][OTf]$ and $Ag(bpy)(TFA)_2$ complexes to activate trifluoroacetate (TFA) by visible-light-induced homolysis. The resulting trifluoromethyl radicals may react with a variety of arenes to forge $C(sp^2)–CF_3$ bonds. This methodology is general and extends to other perfluoroalkyl carboxylates of higher chain length ($R_FCO_2^-$; $R_F = CF_2CF_3$ or $CF_2CF_2CF_3$). The photoredox reaction may be rendered electrophotocatalytic by regenerating the Ag(II) complexes electrochemically during irradiation. Electrophotocatalytic perfluoroalkylation of arenes at turnover numbers exceeding 20 is accomplished by photoexciting the Ag(II)–TFA ligand-to-metal charge transfer (LMCT) state followed by electrochemical re-oxidation of the Ag(I) photoproduct back to the Ag(II) photoreactant.

One-Sentence Summary: Ligand-to-metal charge transfer excitation of electrophilic Ag(II) complexes coupled to electrochemical oxidation provides entry to a potent electrophotocatalytic method for the perfluoroalkylation of arenes.

Photoredox methodologies have emerged as indispensable tools in organic synthesis, employing photons as a clean and selective source of energy to drive challenging chemical reactions under relatively mild conditions (*1*). Of the various photoredox strategies, ligand-to-metal charge transfer (LMCT) processes have been exploited for the generation of reactive intermediates from inert substrates (*2,3*). As LMCT processes involve the transfer of electron density to the metal center, typically only electrophilic metals in higher-valent oxidation states engage in LMCT photochemistry. A variety of complexed metal ions including Cu(II) (*4,5*), Co(III) (*6,7*), Fe(III) (*8,9*), Ni(III) (*10–12*), V(V) (*13*) and Ce(IV) (*14–16*) centers photochemically generate open-shell intermediates upon LMCT excitation (Fig. 1), including chlorine, azidyl, alkoxy, acyl, and alkyl radicals generated from the homolysis of M–Cl (*8,11,12,16*), –N_3 (*5,9*), –OR (*15*), –COR (*7*), and –R (R = alkyl) (*6*) bonds. In addition, photolysis of M–O_2CR bonds is known to induce decarboxylation of the generated carboxyl radical which can provide a source of alkyl or aryl radicals (*4,14*,*17,18*). Noticeably absent from the palette of electrophilic metals is Ag(II). While Ag(I) is a strong oxidant ($E°$ = 0.799 V vs NHE), Ag(II) with its d^9 electronic configuration wields even greater oxidative power ($E°$ = 1.980 V vs NHE) (*19*) by virtue of the hole in its 4d subshell (*20*). As schematically shown in Fig. 1, we envisioned that filling this hole by visible light excitation of the LMCT transition would position the underutilized Ag(II) metal center as a potent photo-oxidant for the activation of challenging substrates.

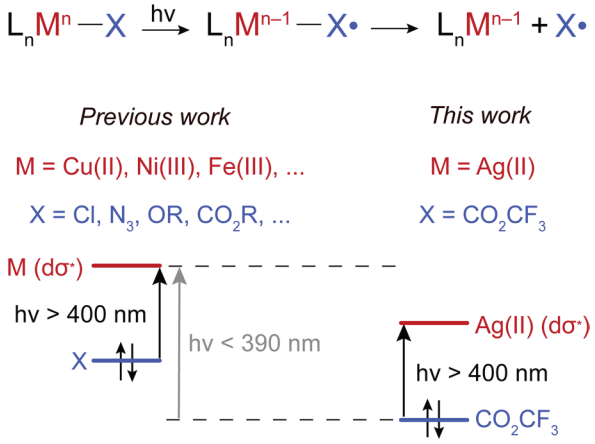

Fig. 1. LMCT chemistry of molecular compounds. Comparison of LMCT photochemistry of typical metal centers versus the highly electrophilic Ag(II) center.

We targeted trifluoroacetate (TFA) as it is an ideal source of the pharmaceutically relevant trifluoromethyl group (*21*), which imparts dramatically enhanced pharmacokinetic properties to drug molecules (*22*). As compared to common CF_3 sources such as the Ruppert–Prakash or Umemoto reagents (*23*), TFA is an ideal CF_3 source due to its low cost and high annual production (*24*). However, the demanding oxidation potential of TFA (>2.2 V vs SCE (*25*)) necessitates forcing conditions for the liberation of its CF_3 group. Thus, previous methods for the decarboxylation of TFA have required either high-energy ultraviolet (UV) irradiation (TiO_2 catalyst, λ_{exc} < 365 nm) (*26,27*), high temperatures (T > 120 °C with Ag salts (*28*) or T > 140 °C with Cu salts (*29*)), or harsh chemical oxidants such as XeF_2 (*30*). Other strategies rely on the pre-activation of TFA or trifluoroacetic anhydride with exogenous reactants such as pyridine *N*-oxides (*31*), sulfoxides (*32*), or hypervalent iodine reagents (*33*) in order to effectively lower the redox potential of TFA within range of traditional photocatalysts. Although functionalization of alkyl carboxylates with *N*-hydroxyphthalimide to form *N*-acyloxyphthalimides allows for the reductive

fragmentation of the N–O bond under mild conditions to liberate carbon dioxide (CO_2) and an alkyl radical, when TFA is employed, the strongly electron withdrawing CF_3 group biases the reductive fragmentation towards the generation of an N-centered radical and the TFA anion leading to amination rather than the desired trifluoromethylation (*34*). Direct Kolbe-type electrolysis of TFA requires large operating cell potentials and the employment of oxidatively resistant substrates; even with unactivated arenes such as benzene, competitive electrochemical oxidation of the arene leads to trifluoroacetoxylation side products (PhO_2CCF_3) in addition to the desired trifluoromethylated aromatics ($PhCF_3$) (*35*). LMCT excitation of well-defined Ag(II)–TFA complexes with visible light would represent a milder and more chemoselective pathway for harnessing the trifluoromethyl group from the redox-reticent TFA substrate.

We now report the synthesis, isolation, and structural characterization of $[Ag(bpy)_2][OTf]_2$ and $[Ag(bpy)_n(O_2CCF_3)_m][OTf]_{2-m}$ (bpy = 2,2′-bipyridine, OTf = CF_3SO_3) complexes. Photolysis of these Ag(II)–TFA complexes with light at wavelengths $\lambda_{exc} > 400$ nm results in rapid decarboxylation to generate trifluoromethyl radicals with the concomitant extrusion of CO_2. We extend this methodology to perfluoroalkyl carboxylates of higher chain length ($R_FCO_2^-$; R_F = CF_2CF_3, $CF_2CF_2CF_3$), demonstrating the generality of this platform. The suite of Ag(II)–CO_2R_F complexes are shown to be competent perfluoroalkylating agents of arenes. By performing the photochemistry under an applied potential ($E_{appl} > E^0$(Ag(II/I)), the system may be turned over catalytically. The electrophotocatalytic perfluoroalkylation of a variety of (hetero)arenes is demonstrated with low Ag loadings and turnover numbers exceeding 20. While electrophotocatalytic C–H trifluoromethylation has been accomplished previously using the Langlois reagent (NaO_2SCF_3) as a specialized CF_3 source due to its accessible oxidation potential (*36*), the described Ag(II)-mediated electrophotocatalytic system enables the direct use of TFA. Whereas the work described herein highlights the activation of TFA, our results suggest that molecular Ag(II) complexes are superior, yet underutilized, super-oxidizing catalysts that are capable of activating a variety of inert substrates using visible light.

Synthesis and characterization of Ag(II) complexes. Addition of AgO to a solution of bpy in aqueous triflic acid (50% v/v) gives a deep red solution that furnishes $[Ag(bpy)_2][OTf]_2$ (**1**$[OTf]_2$) as a red microcrystalline powder upon precipitation with water. The tetrafluoroborate salt, **1**$[BF_4]_2$, may be prepared similarly by replacing triflic acid with terafluoroboric acid. The synthesis can be performed on a multi-gram scale (8 mmol) and **1**$[OTf]_2$ is isolated in 64% yield. We note that **1**$[OTf]_2$ has been synthesized previously, requiring either a multi-step electrochemical synthesis or one-pot procedures that give impure product or low yields, and the compound has not been structurally characterized (*37*). Unique among other known Ag(II) molecular complexes is the solubility of **1**$[OTf]_2$ or **1**$[BF_4]_2$ in organic solvents, allowing us to avoid aqueous solution and thus circumvent the oxidation of water. Dissolution of the isolable microcrystalline powder in acetonitrile (MeCN) followed by vapor diffusion of benzene resulted in the formation of deep red crystals. Crystal structure analysis reveals Ag(II) to reside in a tetragonally distorted bpy ligand field (Fig. 2A). **1**$[OTf]_2$ is characterized by an EPR signal that is an axial doublet (fig. S1) and an effective magnetic moment of 1.97 μ_B, consistent with a d^9 ground state.

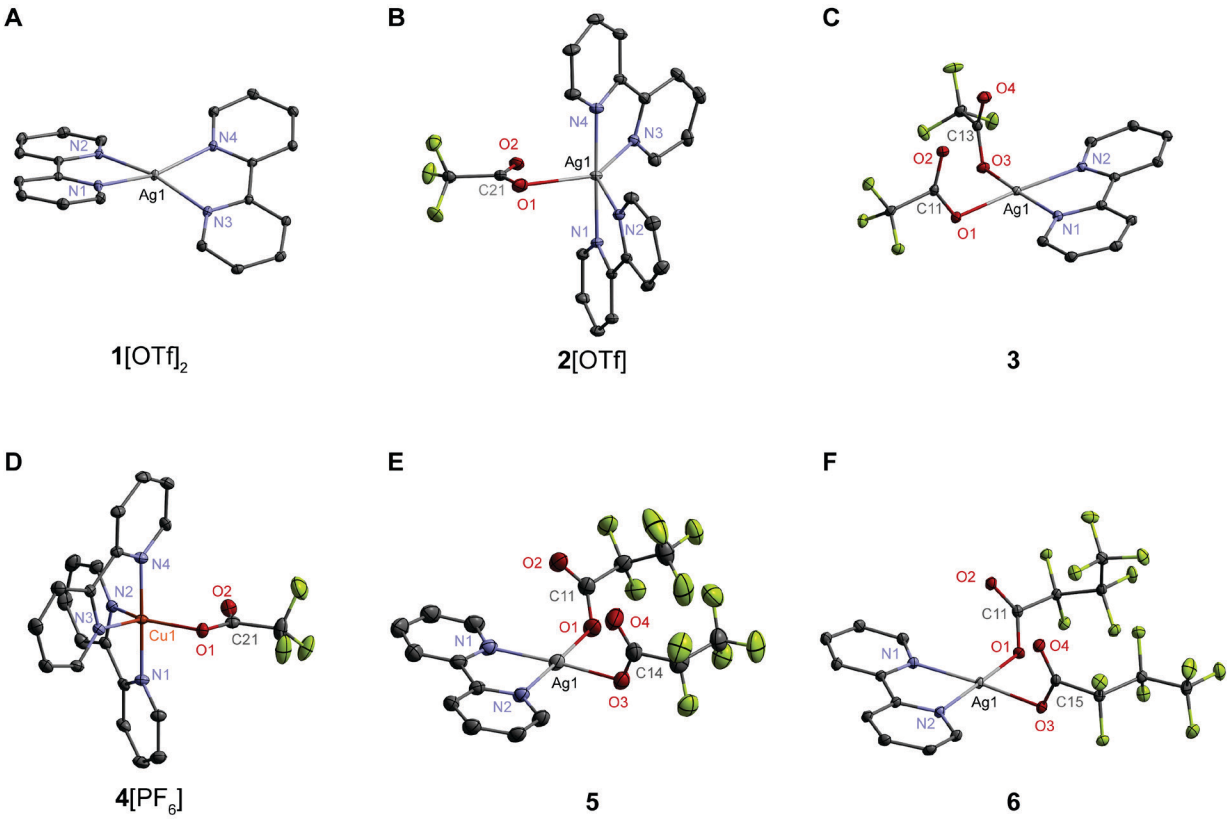

Fig. 2. **Crystal structures of Ag(II) complexes and a Cu(II) congener.** Atomic displacement parameter plot of (**A**) **1**$[OTf]_2$ at 15 K, (**B**) **2**[OTf] at 15 K, (**C**) **3** at 15 K, (**D**) **4**$[PF_6]$ at 100 K, (**E**) **5** at 100 K and (**F**) **6** at 15 K, drawn at 50% probability level as ascertained by single-crystal X-ray diffraction analysis. Color scheme for structures **1**–**6**: Ag (light gray), Cu (dark orange), F (yellow green), O (red), N (blue), C (dark gray). Counterions, hydrogen atoms, and solvent molecules omitted for clarity. Selected crystallographic bond metrics are provided in Table S3.

Treatment of a slurry of **1**$[OTf]_2$ in dichloromethane (CH_2Cl_2) with bis(triphenylphosphine)iminium trifluoroacetate ([PPN][TFA]) leads to the introduction of TFA into the primary coordination sphere of Ag(II). **1**$[OTf]_2$ reacts with one equivalent of [PPN][TFA] in the presence of an additional equivalent of bpy to furnish a solid which may be crystallized as black needles by layering CH_2Cl_2 solutions with pentane at –36 °C. The crystal structure establishes $[Ag(bpy)_2(O_2CCF_3)][OTf]$ (**2**[OTf]) (Fig. 2B), obtained in 48% yield, as a rare example of Ag(II) in a distorted trigonal bipyramidal ligand field in which TFA binds via essentially a κ^1 coordination mode (d(Ag–O1) = 2.4814(15) Å, d(Ag–O2) = 2.7104(14) Å). The bpy ligands in **2**[OTf] distort to assume a nearly linear axial N1–Ag–N4 bond angle of 178.65(5)° in order to accommodate TFA in the primary coordination sphere. The relative similarity in the C21–O1 and C21–O2 bond distances in the TFA ligand point to delocalization of the negative charge on the carboxylate group. When a slurry of **1**$[OTf]_2$ in CH_2Cl_2 is treated with excess [PPN][TFA], the orange solid $Ag(bpy)(O_2CCF_3)_2$ (**3**) (Fig. 2C), in which one bpy ligand in **1**$[OTf]_2$ is substituted by two monodentate TFA ligands, is obtained in 59% yield. The neutral square planar coordination geometry draws similarities to Ag(4,4′-dimethyl-bpy)$(NO_3)_2$ in which nitrate anions serve as anionic ligands (*38*). **3** packs in the crystalline lattice as sets of symmetrically equivalent dimers, forming diamond-core like structures with a weak apical Ag···O interaction. Both **2**[OTf] and **3**

show no resolvable ^{1}H NMR signals for bpy due to paramagnetic broadening. The compounds display axial EPR signals consistent with a paramagnetic S = ½ ground state (fig. S1), which is consistent with effective magnetic moments of 2.06 (**2**[OTf]) and 1.78 (**3**) μ_B. **3** is ^{19}F NMR silent while **2**[OTf] displays a single resonance corresponding to unbound triflate.

LMCT photogeneration of CF_3 radical from Ag(II)–TFA complexes. LMCT photochemistry of **2**[OTf] and **3** was accessed using visible light. Photolysis (λ_{exc} = 450 nm) of **2**[OTf] in MeCN at 21.3 °C resulted in the complete bleaching of all visible absorption features within 30 min whereas **3** exhibits growth of a band at 700 nm that disappears upon continued irradiation (Figs. 3A and 3B); under identical conditions, **1**[OTf]$_2$ was found to be photostable as compared to **2**[OTf] and **3** (fig. S2). Compound **2**[OTf] converts to **3** with excess TFA, and similarly the addition of excess bpy to **3** results in conversion to **2**[OTf] (fig. S3). Thus, in the case of **3**, we believe that there is an initial equilibrium established between **2**[OTf] and **3**, thus accounting for the initial appearance of the 700 nm absorption band in Fig. 3B. The loss of absorption bands in the visible spectral region as well as the disappearance of the initial axial EPR signal of **2**[OTf] and **3** with irradiation (fig. S4) are consistent with the photoreduction of the Ag(II) center to form the d^{10} Ag(I). Additionally, the ^{1}H NMR signals of Ag(I) bpy complexes appear over the time course of photolysis. For **3**, clean conversion to the trigonal planar Ag(I)(bpy)(TFA) complex (*39*) is observed after photolysis via ^{1}H NMR and UV-vis spectroscopy (fig. S5). Concomitant to the formation of Ag(I), photoinduced cleavage of the Ag(II)–TFA bond should furnish the TFA radical (TFA•), decarboxylation of which to yield CO_2 and CF_3• is highly exergonic (*40*).

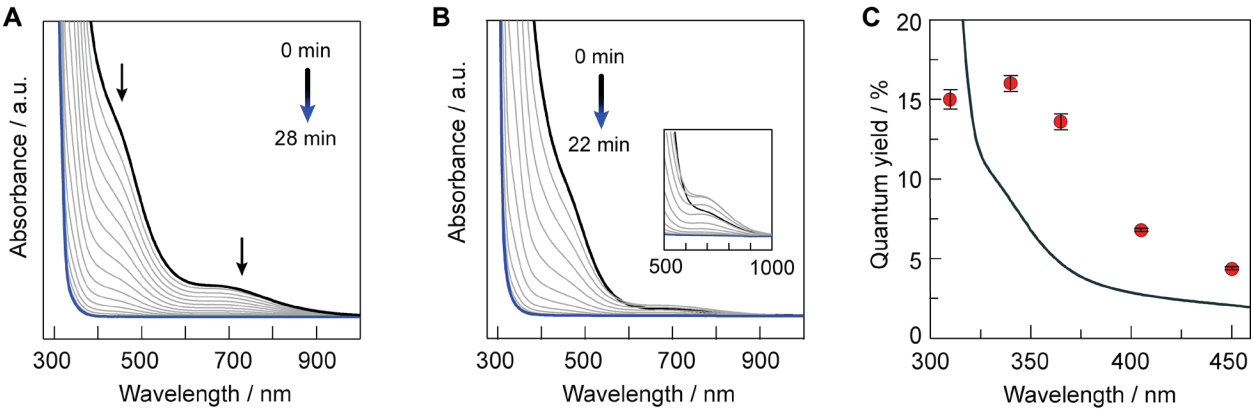

Fig. 3. **LMCT photochemistry of Ag(II) complexes.** Steady-state photolysis of 1 mM solutions of (**A**) **2**[OTf] and (**B**) **3** in MeCN under 450 nm irradiation at 21.3 °C. Spectra were recorded at 2 min intervals. (**C**) Action spectrum of **2**[OTf]; quantum yields (red circles) are superimposed on the UV spectrum of **2**[OTf] (black line) with error bars determined from the least squares fit of the photolytic conversion at different time points.

The decarboxylation of TFA• to CO_2 was observed by steady-state and time-resolved vibrational spectroscopy. Fig. 4A shows the steady-state IR spectrum of photolyzed solutions of **3**. Signals associated with the TFA ligand in **3** (asymmetric and symmetric carboxyl stretches at 1693 and 1408 cm^{-1}, respectively) and CF_3 (1196 cm^{-1}) disappear upon irradiation of solutions of **3** with the concomitant growth of the vibrational signature of CO_2 (2341 cm^{-1}). A similar decarboxylation process is observed for photolyzed solutions of **2**[OTf] (fig. S6). Figure 4C shows the time-resolved infrared (TRIR) spectrum upon laser excitation of **3**. On a nanosecond timescale, bleach

signals are observed due to the disappearance of the asymmetric carboxyl and CF_3 stretching vibrations of TFA with the concomitant growth of CO_2. The time evolution of the vibrational signatures in Fig. 4C approaches the instrument response function, placing a lower limit of $k > 2.5 \times 10^7$ s^{-1} for TFA• decarboxylation.

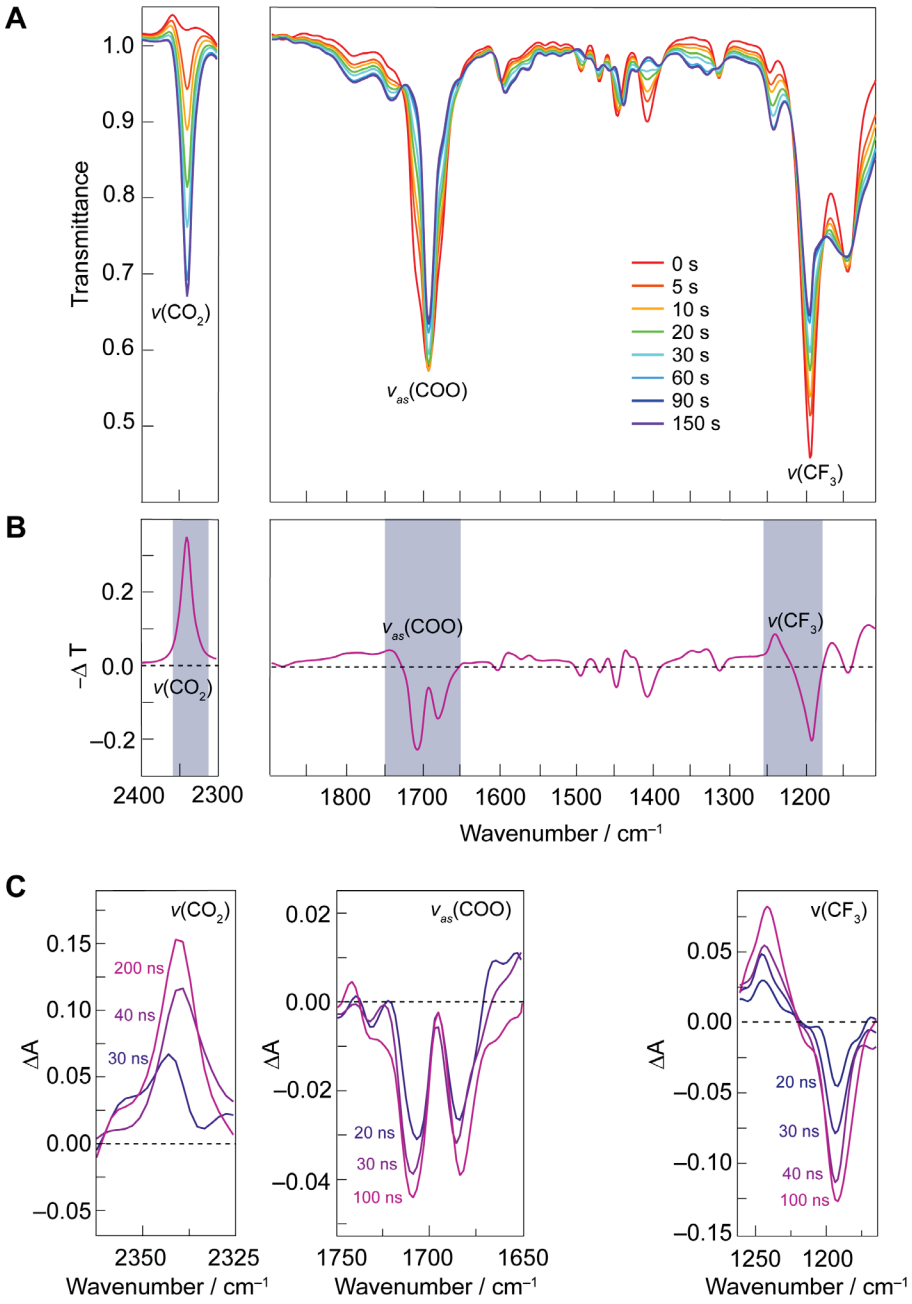

Fig. 4. Steady-state and time-resolved infrared spectra of photolyzed solutions of 3. (**A**) Steady state FTIR spectral changes of a photolyzed solution (λ_{exc} = 467) of **3** in CD_3CN. (**B**) Difference spectrum of FTIR traces in (**A**) recorded at 150 s and 0 s of irradiation. (**C**) Time resolved infrared spectra measured in the energy ranges indicated by the shaded boxes in (**B**).

The decarboxylation of TFA• to CF_3• was established with ^{19}F NMR spectroscopy. Photolysis of **2**[OTf] generates CF_3• radicals, which react with bpy ligands in the absence of a substrate to produce CF_3-derivatized bpy and with solvent to produce fluoroform (in MeCN), fluoroform-D (in CD_3CN), and chlorotrifluoromethane (in CH_2Cl_2) (fig. S7). We note that heating (60 °C) either **2**[OTf] or **3** in CD_3CN solutions protected from ambient light does not produce Ag(I) or CF_3• as ascertained by ^1H and ^{19}F NMR spectroscopy, respectively (fig. S8).

The importance of Ag(II) in mediating the challenging decarboxylation of TFA via LMCT excitation is revealed by a comparative study using the less electrophilic Cu(II) center in the same ligand field afforded by $[Cu(bpy)_2(TFA)][PF_6]$ (**4**[PF_6]). The solid-state structure of **4**[PF_6] (Fig. 2D) is similar to **2**[OTf] with the TFA ligand engaging in a shorter contact to the Cu center (d(Cu–O1) = 2.0703(19) Å). Irradiation of **4**[PF_6] with λ_{exc} = 370 nm in CD_3CN exhibits no observable changes as monitored by UV-vis-NIR, ^{19}F NMR, and FTIR spectroscopies (fig. S9).

Reactivity of photogenerated perfluoroalkyl radicals. The CF_3• radical readily reacts with arenes to form $C(sp^2)$–CF_3 linkages. Photolysis of **2**[OTf] in the presence of excess benzene (75 equiv) results in the formation of trifluorotoluene ($PhCF_3$) (36%) and a mixture of TFA and trifluoroacetic acid (TFAH) (52%), as was confirmed by spiking samples with either [PPN][TFA] or TFAH (fig. S10). The generation of approximately half an equivalent of $PhCF_3$ for each equivalent of **2**[OTf] suggests that after radical addition of CF_3• to benzene, the resultant arene radical is oxidized by a second equivalent of Ag(II) with TFA acting as a base to furnish $PhCF_3$ and TFAH (Fig. 5). As shown by the action spectrum in Fig. 3C, the photoreaction quantum yield of **2**[OTf] as ascertained by ferrioxalate actinometry is appreciable; the increase and levelling of the quantum yield with wavelength (4.2%, 6.8% and 14.9% at 450, 405 and 340 nm, respectively) establishes the energy of the LMCT transition to occur at ~350 nm; similar photochemistry and quantum efficiency trends were observed for **3**. We note that the isolation of **2**[OTf] (or **3**) is not necessary to perform perfluoroalkylations. The **1**$[OTf]_2$ complex competently binds $R_FCO_2^-$ in situ to provide entry into the LMCT photochemistry. Irradiating (450 nm) a mixture containing Na(TFA) as the limiting reagent (12.5 mM) and 2 equiv of **1**$[OTf]_2$ in combination with one equivalent of benzene for 1 h produced $PhCF_3$ in 27% yield, as detected by ^{19}F NMR spectroscopy and gas chromatography (GC). The remainder of the mass balance can be ascribed to H-atom abstraction of the solvent by CF_3• to produce fluoroform as a byproduct as well as the trifluoromethylation of bpy ligands as opposed to the benzene substrate (fig. S7). The side reactions of CF_3• may be minimized by performing the photolysis with excess substrate; the $PhCF_3$ yield increases to 78% upon using 20 equiv of benzene (fig. S11). No $PhCF_3$ is observed upon irradiation of **1**$[OTf]_2$ with benzene in the absence of a TFA source (fig. S12).

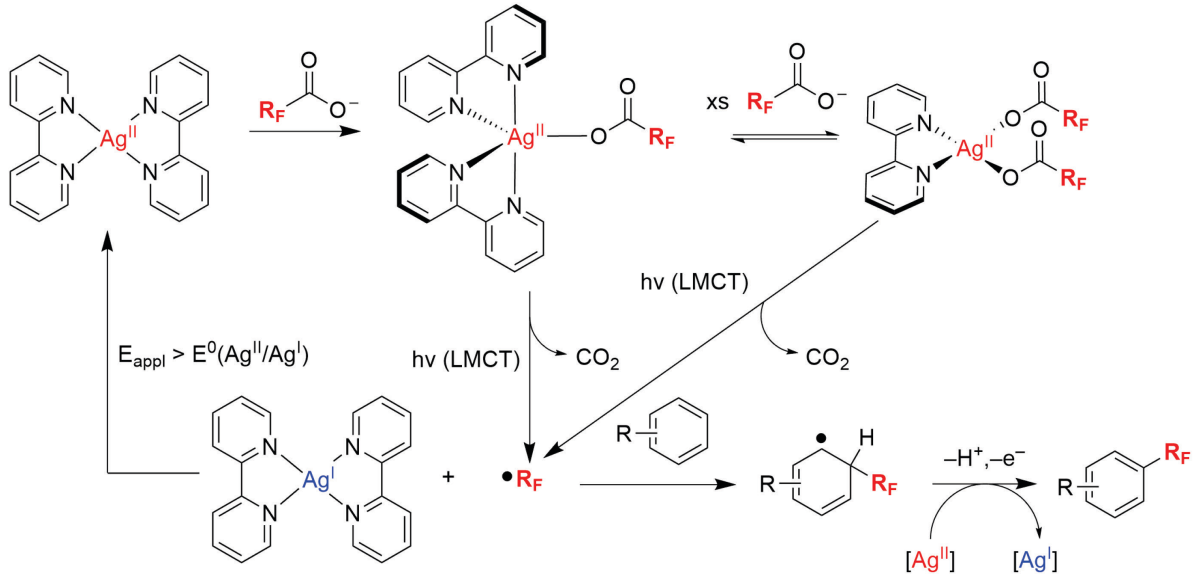

Fig. 5. **Photo-/electro- chemical reaction mechanism**. Mechanism of Ag(II)-mediated perfluoroalkylation of arenes via LMCT excitation under an applied potential to engender a catalytic cycle.

As shown in Fig. 6 a variety of arenes as well as heteroarenes such as 1-methylpyrazole are compatible and trifluoromethylated aromatic compounds may be produced in moderate to high yields with LMCT irradiation of **1**$[OTf]_2$ in the presence of TFA. The use of an inorganic base (K_2HPO_4) does not significantly alter reaction yields. The observed product ratios for chlorobenzene, methyl benzoate, 4-chloroanisole, methyl 4-chlorobenzoate, 1-methylpyrazole, and benzamide reflect the radical nature of the reaction. Interestingly, pre-saturating the reaction mixture with O_2 prior to irradiation led to trifluoromethoxylation, as evidenced by the production of (trifluoromethoxy)benzene when O_2 is present. The trifluoromethoxy group is an important motif in pharmaceutical chemistry, yet trifluoromethoxylation reactions remain underdeveloped and relatively few radical-based trifluoromethoxylations have been reported (*41*,*42*). The mechanism of this novel O_2/Ag(II)-mediated radical trifluoromethoxylation is currently under study.

To further demonstrate the generality of the current approach, perfluoro groups beyond the parent CF_3 group may be installed. Such higher order perfluoroalkylations are important to pharmaceutical chemistry, though with far fewer demonstrations as compared to trifluoromethylations (*43*). Single crystals of Ag(bpy)$(O_2CCF_2CF_3)_2$ (**5**) and Ag(bpy)$(O_2CCF_2CF_2CF_3)_2$ (**6**) were obtained, and these compounds were shown to be structural analogs to **3** (Figs. 2E and 2F). Photoinduced perfluoroalkylations of benzene could be performed by irradiating solutions of **1**$[OTf]_2$ with the sodium salts of pentafluoropropionate and heptafluorobutyrate (Fig. 6).

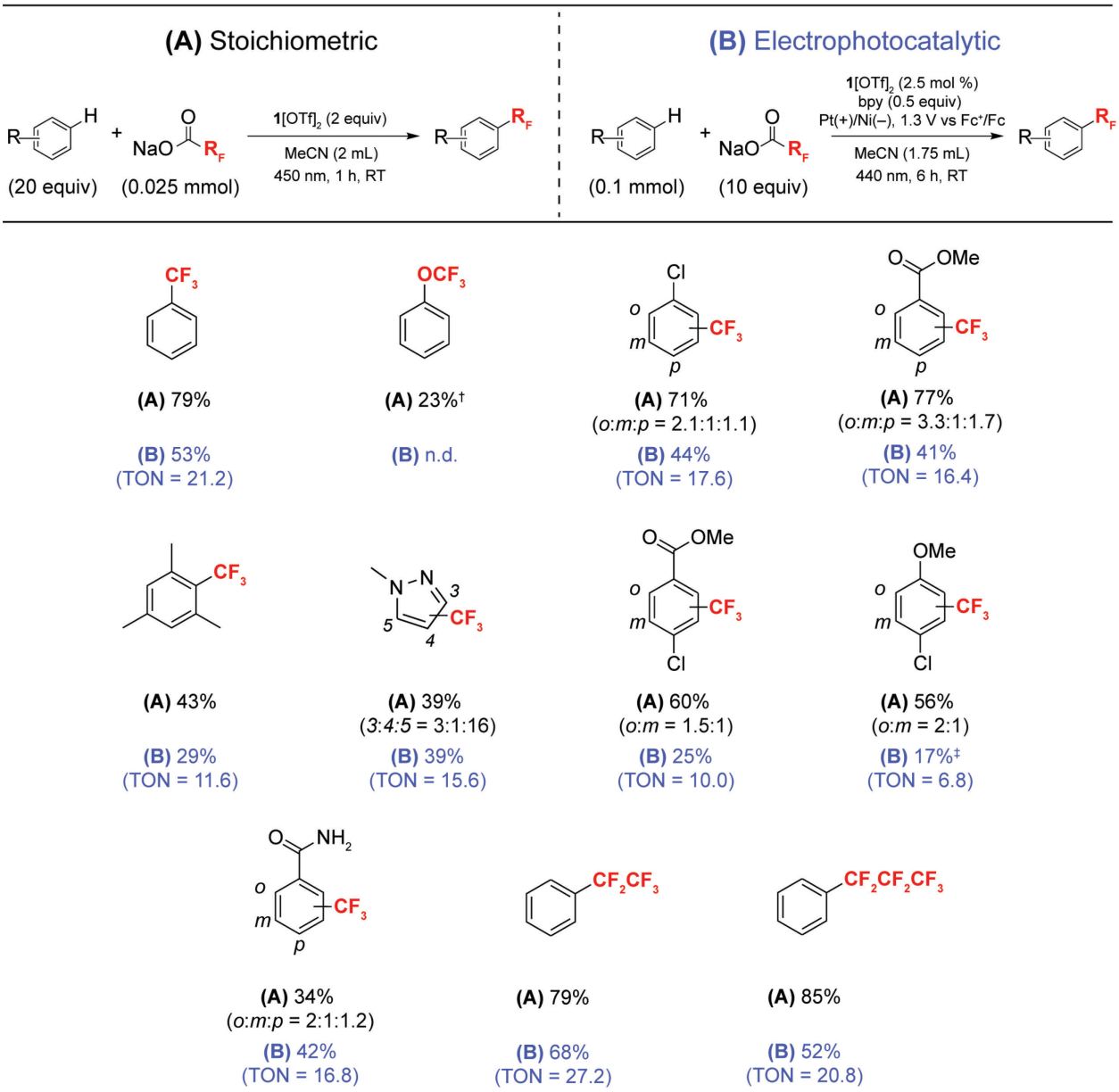

Fig. 6. Ag(II)-mediated trifluoromethylation of arenes.**Yields for trifluoromethylated products determined by ^{19}F NMR spectroscopy. †Solution was saturated with O_2 prior to irradiation, reaction time: 6 h. ‡Electrophotocatalysis performed at 1.1 V vs Fc^+/Fc.

Electrophotocatalysis. The photoredox reaction may be rendered electrophotocatalytic by regenerating **1**[OTf] electrochemically during irradiation (Fig. 5). Cyclic voltammetry reveals a reversible one-electron redox wave for **1**$[OTf]_2$ at E^0 = 930 mV vs ferrocenium/ferrocene (Fc^+/Fc) (fig. S13). The trifluoromethylation of benzene was thus achieved with 21.2 turnovers upon performing the photoredox reaction (λ_{exc} = 440 nm) with 2.5 mol % **1**$[OTf]_2$, 0.5 equiv of bpy, 1 equiv of benzene, and 10 equiv of Na(TFA) in a three-electrode divided cell under an applied bias of 1.3 V vs Fc^+/Fc. Bis(trifluoromethylated) benzene products were also observed in 11% yield. Of note is the absence of phenyl trifluoroacetate (PhO_2CCF_3) side product in the reaction mixture, which arises from the direct oxidation of benzene (*35*). This highlights the mildness of this

electrophotocatalytic method, as oxidation of arenes is avoided in contrast to direct electrolysis methods. Additionally, the lack of this side-product is consonant with the TRIR measurements, which establishes that the short-lived TFA radical will decarboxylate before diffusing to arene substrates. Extension of the electrophotocatalytic method to the pentafluoroethylation and heptafluoropropylation of benzene resulted in similar reaction efficiency (27.2 and 20.8 turnovers, respectively). Application of the electrophotocatalysis to other arenes resulted in their successful, catalytic trifluoromethylation with moderate turnover numbers. Any potential anodic of the Ag(II/I) couple but cathodic of the substrate oxidation potential may be applied. Figure S14 shows the permissible potential window for electrophotocatalysis of substrates with oxidation potentials more anodic than TFA. In the case of chloroanisole, the reaction was run at an applied potential of 1.1 V vs Fc^{+}/Fc to avoid direct oxidation of the electron-rich substrate.

We have detailed a new electrophotoredox method to deliver perfluoroalkyl radicals to arenes utilizing the LMCT photochemistry of Ag(II) coupled to Ag(I) oxidation. The homolysis of the Ag(II)–O_2CR_F bond smoothly leads to Ag(I) and the perfluoroalkyl radical, which may be harnessed for C(sp^2)–CF_3 bond formations. The high electrophilicity of the Ag(II) center is essential for generating perfluoroalkyl radicals from their corresponding carboxylates under mild photochemical conditions (*44*,*45*). The electrophotoredox method described herein is direct and requires only visible light to drive the LMCT activation of TFA or higher perfluoroalkyl carboxylates without the need for the pre-functionalization of TFA or using the forcing potentials for Kolbe electrolysis. By performing the LMCT photochemistry under electrochemical conditions in which Ag(I) is re-oxidized to Ag(II), an electrophotocatalytic cycle may be established where perfluoroalkyl carboxylates are directly employed as perfluoroalkylating agents under mild conditions. Considering the inertness of perfluoroalkyl carboxylates towards oxidation, the chemistry described herein may be generalized to a variety of inert substrates that are capable of ligating to a Ag(II) center.

References and Notes

1. M. H. Shaw, J. Twilton, D. W. C. MacMillan, Photoredox Catalysis in Organic Chemistry. *J. Org. Chem.* **81**, 6898–6926 (2016).
2. F. Juliá, Ligand-to-Metal Charge Transfer (LMCT) Photochemistry at 3d-Metal Complexes: An Emerging Tool for Sustainable Organic Synthesis. *ChemCatChem* **14**, e202200916 (2022).
3. Y. Abderrazak, A. Bhattacharyya, O. Reiser, Visible-Light-Induced Homolysis of Earth-Abundant Metal-Substrate Complexes: A Complementary Activation Strategy in Photoredox Catalysis. *Angew. Chem. Int. Ed.* **60**, 21100–21115 (2021).
4. A. Reichle, H. Sterzel, P. Kreitmeier, R. Fayad, F. Mn. Castellano, J. Rehbein, O. Reiser, Copper(II)-Photocatalyzed Decarboxylative Oxygenation of Carboxylic Acids. *Chem. Commun.* **58**, 4456–4459 (2022).
5. A. Hossain, A. Vidyasagar, C. Eichinger, C. Lankes, J. Phan, J. Rehbein, O. Reiser, Visible-Light-Accelerated Copper(II)-Catalyzed Regio- and Chemoselective Oxo-Azidation of Vinyl Arenes. *Angew. Chem. Int. Ed.* **57**, 8288–8292 (2018).
6. M. E. Weiss, L. M. Kreis, A. Lauber, E. M. Carreira, Cobalt-Catalyzed Coupling of Alkyl Iodides with Alkenes: Deprotonation of Hydridocobalt Enables Turnover. *Angew. Chem. Int. Ed.* **50**, 11125–11128 (2011).

7. M. Ociepa, O. Baka, J. Narodowiec, D. Gryko, Light-Driven Vitamin B_{12}-Catalysed Generation of Acyl Radicals from 2-S-Pyridyl Thioesters. *Adv. Synth. Catal.* **359**, 3560–3565 (2017).
8. Gonzalez, M. I.; Gygi, D.; Qin, Y.; Zhu, Q.; Johnson, E. J.; Chen, Y.-S.; Nocera, D. G. Taming the Chlorine Radical: Enforcing Steric Control over Chlorine-Radical-Mediated C–H Activation. *J. Am. Chem. Soc.* **144**, 1464–1472 (2022).
9. Bian, K.-J.; Kao, S.-C.; Nemoto, D.; Chen, X.-W.; West, J. G. Photochemical Diazidation of Alkenes Enabled by Ligand-to-Metal Charge Transfer and Radical Ligand Transfer. *Nat. Commun.* **13**, 7881 (2022).
10. S. K. Kariofillis, A. G. Doyle, Synthetic and Mechanistic Implications of Chlorine Photoelimination in Nickel/Photoredox C(sp^3)–H Cross-Coupling. *Acc. Chem. Res.* **54**, 988–1000 (2021).
11. S. J. Hwang, D. C. Powers, A. G. Maher, B. L. Anderson, R. G. Hadt, S.-L. Zheng, Y.-S. Chen, D. G. Nocera, Trap-Free Halogen Photoelimination from Mononuclear Ni(III) Complexes. *J. Am. Chem. Soc.* **137**, 6472–6475 (2015).
12. S. J. Hwang, B. L. Anderson, D. C. Powers, A. G. Maher, R. G. Hadt, D. G. Nocera, Halogen Photoelimination from Monomeric Nickel(III) Complexes Enabled by the Secondary Coordination Sphere. *Organometallics* **34**, 4766–4774 (2015).
13. S. M. Aliwi, C. H. Bamford, Photoinitiation of Free-Radical Polymerization by Vanadium Chelates. Part 3. Methoxo-Oxobis(8-Quinolyloxo)Vanadium(V). *J. Chem. Soc. Faraday Trans. 1* **71**, 1733–1743 (1975).
14. S. Shirase, S. Tamaki, K. Shinohara, K. Hirosawa, H. Tsurugi, T Satoh, K. Mashima, Cerium(IV) Carboxylate Photocatalyst for Catalytic Radical Formation from Carboxylic Acids: Decarboxylative Oxygenation of Aliphatic Carboxylic Acids and Lactonization of Aromatic Carboxylic Acids. *J. Am. Chem. Soc.* **142**, 5668–5675 (2020).
15. A. Hu, J.-J. Guo, H. Pan, Z. Zuo, Selective Functionalization of Methane, Ethane, and Higher Alkanes by Cerium Photocatalysis. *Science* **361**, 668–672 (2018).
16. Q. Yang, Y. H. Wang, Y. Qiao, M. Gau, P. J. Carroll, P. J. Walsh, E. J. Schelter, Photocatalytic C–H Activation and the Subtle Role of Chlorine Radical Complexation in Reactivity. *Science* **372**, 847–852 (2021).
17. G. A. Lutovsky, S. N. Gockel, M. W. Bundesmann, S. W Bagley, T. P. Yoon, Iron-Mediated Modular Decarboxylative Cross-Nucleophile Coupling. *Chem*, **9**, 1610-1621 (2023).
18. S. B. Beil, T. Q. Chen, N. E. Intermaggio, D. W. C. MacMillan, Carboxylic Acids as Adaptive Functional Groups in Metallaphotoredox Catalysis. *Acc. Chem. Res.* **55**, 3481–3494 (2022).
19. G. V. Zhutaeva, N. A. Shumilova, Copper, Silver, and Gold, in *Standard Potentials in Aqueous Solutions*, A. J. Bard, R. Parsons, J. Jordan, Eds. (Marcel Dekker, 1985) Ch 11, pp 294–313.
20. W. Grochala, Z. Mazej, Chemistry of Silver(II): A Cornucopia of Peculiarities. *Phil. Trans. R. Soc. A* **373**, 20140179 (2015).
21. O. A. Tomashenko, V. V. Grushin, Aromatic Trifluoromethylation with Metal Complexes. *Chem. Rev.* **111**, 4475–4521 (2011).
22. K. Müller, C. Faeh, F. Diederich, Fluorine in Pharmaceuticals: Looking Beyond Intuition. *Science* **317**, 1881–1886 (2007).
23. K. A. McReynolds, R. S. Lewis, L. K. G. Ackerman, G. G. Dubinina, W. Brennessel, D. A. Vicic, Decarboxylative Trifluoromethylation of Aryl Halides Using Well-Defined Copper–Trifluoroacetate and –Chlorodifluoroacetate Precursors. *J. Fluor. Chem.* **131**, 1108–1112 (2010).

24. S. E. López, J. Salazar, Trifluoroacetic Acid: Uses and Recent Applications in Organic Synthesis. *J. Fluor. Chem.* **156**, 73–100 (2013).
25. C. Depecker, H. Marzouk,a S. Trevin and J. Devynck, Trifluoromethylation of Aromatic Compounds via Kolbe Electrolysis in Pure Organic Solvent. Study on Laboratory and Pilot Scale. *New J. Chem.* **23**, 739–742 (1999).
26. J. Lin, Z. Li, J. Kan, S. Huang, W. Su, Y. Li, Photo-Driven Redox-Neutral Decarboxylative Carbon-Hydrogen Trifluoromethylation of (Hetero)Arenes with Trifluoroacetic Acid. *Nat. Commun.* **8**, 14353 (2017).
27. C. Lai, T. E. Mallouk, A New Approach to the Photochemical Trifluoromethylation of Aromatic Compounds. *J. Chem. Soc. Chem. Commun.* 1359–1361 (1993).
28. G. Shi, C. Shao, S. Pan, J. Yu, Y. Zhang, Silver-Catalyzed C–H Trifluoromethylation of Arenes Using Trifluoroacetic Acid as the Trifluoromethylating Reagent. *Org. Lett.* **17**, 38–41 (2015).
29. D. Staveness, I. Bosque, C. R. J. Stephenson, Free Radical Chemistry Enabled by Visible Light-Induced Electron Transfer. *Acc. Chem. Res.* **49**, 2295–2306 (2016).
30. Y. Tanabe, N. Matsuo, N. Ohno, Direct Perfluoroalkylation including Trifluoromethylation of Aromatics with Perfluoro Carboxylic Acids Mediated by Xenon Difluoride. *J. Org. Chem.* **53**, 4582–4585 (1988).
31. J. W. Beatty, J. J. Douglas, K. P. Cole, C. R. J. Stephenson, A Scalable and Operationally Simple Radical Trifluoromethylation. *Nat. Commun.* **6**, 7919 (2015).
32. D. Yin, D. Su, J. Jin, Photoredox Catalytic Trifluoromethylation and Perfluoroalkylation of Arenes Using Trifluoroacetic and Related Carboxylic Acids. *Cell Rep. Phys. Sci.* **1**, 100141 (2020).
33. B. Yang, D. Yu, X-H. Xu, F-L. Qing, Visible-Light Photoredox Decarboxylation of Perfluoroarene Iodine(III) Trifluoroacetates for C–H Trifluoromethylation of (Hetero)arenes. *ACS Catal.* **8**, 2839–2843 (2018).
34. L. J. Allen, P. J. Cabrera, M. Lee, M. S. Sanford, *N*-Acyloxyphthalimides as Nitrogen Radical Precursors in the Visible Light Photocatalyzed Room Temperature C–H Amination of Arenes and Heteroarenes. *J. Am. Chem. Soc.* **136**, 5607–5610 (2014).
35. J. Qi, J. Xu, H. T. Ang, B. Wang, N. K. Gupta, S. R. Dubbaka, P. O'Neill, X. Mao, Y. Lum, J. Wu, Electrophotochemical Synthesis Facilitated Trifluoromethylation of Arenes using Trifluoroacetic Acid. *J. Am. Chem. Soc*. **145**, 24965–24971 (2023).
36. Y. Qiu, A. Scheremetjew, L. H. Finger, L. Ackermann, Electrophotocatalytic Undirected C–H Trifluoromethylations of (Het)Arenes. *Chem. Eur. J.* **26**, 3241–3246 (2020).
37. W. G. Thorpe, J. K. Kochi, Silver(II) Complexes of Dipyridyl. *J. Inorg. Nucl. Chem.* **33**, 3958–3962 (1971).
38. S. Kandaiah, E.M. Peters, M. Jansen, Electrocrystallization of Tetra- and Hexa-Coordinated Silver(II) Compounds Based on 4,4′-Dimethyl-2,2′-Bipyridine Ligand – Single Crystal Structures and Magnetic Studies. *Z. Für Anorg. Allg. Chem.* **634**, 2483–2486 (2008).
39. E. Szłyk, Robert Szczęsny, Andrzej Wojtczak, X-ray structural and Gas Phase Studies of Silver(I) Perfluorinated Carboxylate Complexes with 2,2′-Bipyridyl as Potential Precursors for Chemical Vapour Deposition (CVD) *Dalton Trans.* **39**, 1823–1830 (2010).
40. G. dos Passos Gomes, A. Simmer, K. M. Smith, B. König, I. V. Alabugin, CO_2 or SO_2: Should It Stay, or Should It Go? *J. Org. Chem.* **84**, 6232–6243 (2019).
41. Y. Ouyang, X-H. Xu, F-L. Qing, Electrochemical Trifluoromethoxylation of (Hetero)aromatics with a Trifluoromethyl Source and Oxygen. *Angew. Chem. Int. Ed.* **61**, e202114048 (2022).

42. S. Dix, P. Golz, J. R. Schmid, S. Riedel, M. N. Hopkinson, Radical C–H Trifluoromethoxylation of (Hetero)arenes with Bis(trifluoromethyl)peroxide. *Chem. Eur. J.* **27**, 11554–11558 (2021).
43. L. I. Panferova, F. M. Miloserdov, A. Lishchynskyi, M. Martínez Belmonte, J. Benet-Buchholz, V. V. Grushin, Well-Defined CuC_2F_5 Complexes and Pentafluoroethylation of Acid Chlorides. *Angew. Chem. Int. Ed.* **54**, 5218–5222 (2015).
44. During the revision process for this manuscript, alkene hydrotrifluoromethylation by an iron catalyst irradiated with 390-nm light to decarboxylate trifluoroacetate was reported.
45. K.-J. Bian, Y.-C. Lu, D. Nemoto, S.-C. Kao, X. Chen, J. G. West, Photocatalytic Hydrofluoroalkylation of Alkenes with Carboxylic Acids. *Nat. Chem.* doi 10.1038/s41557-023-01365-0 (2023).
46. S. Tyagi, B. Hathaway, S. Kremer, H. Stratemeier, D. Reinen, Crystal Structure of Bis(2,2′-bipyridyl)monochlorocopper(II) Hexafluorophosphate Monohydrate at 298 K and the Electron Spin Resonance Spectra of Some Bis(2,2′-bipyridyl)copper(II) Complexes to 4.2 K. J. *Chem. Soc. Dalton Trans.* 2087–2091 (1984).
47. C. P. Rosenau, B. J. Jelier, A. D. Gossart, A. Togni, Exposing the Origins of Irreproducibility in Fluorine NMR Spectroscopy. *Angew. Chem. Int. Ed.* **57**, 9528–9533 (2018).
48. D. F. Evans, The Determination of the Paramagnetic Susceptibility of Substances in Solution by Nuclear Magnetic Resonance. *J. Chem. Soc.* 2003–2005 (1959).
49. G. A. Bain, J. F. Berry, Diamagnetic Corrections and Pascal's Constants. *J. Chem. Ed.* **85**, 532–536 (2008).
50. D. J. Darensbourg, G. P. Wu, A One-Pot Synthesis of a Triblock Copolymer from Propylene Oxide/Carbon Dioxide and Lactide: Intermediacy of Polyol Initiators. *Angew. Chem. Int. Ed.* **52**, 10602–10606 (2013).
51. G. M. Sheldrick, CELL NOW V2008/2, Bruker AXS (2008).
52. B. A. X. S. Inc., SAINT and APEX 2 Software for CCD Diffractometers, Bruker Analytical X-ray Systems, Inc. (2000).
53. G. M. Sheldrick, TWINABS, Bruker Analytical X-ray Systems (2014).
54. G. M. Sheldrick, SADABS, Bruker Analytical X-ray Systems (2014).
55. G. M. Sheldrick, SHELXT - Integrated Space-Group and Crystal-Structure Determination. *Acta Cryst. A* **71**, 3–8 (2015).
56. G. M. Sheldrick, SHELXL, University of Göttingen, Germany (2014).
57. O. V. Dolomanov, L. J. Bourhis, R. J. Gildea, J. A. K. Howard, H. Puschmann, OLEX2: A Complete Structure Solution, Refinement and Analysis Program. *J. Appl. Cryst*. **42**, 339–341 (2009).
58. P. P. Lampkin, B. J. Thompson S. H. Gellman, Versatile Open-Source Photoreactor Architecture for Photocatalysis Across the Visible Spectrum. *Org. Lett.* **23**, 5277–5281 (2021).
59. C. G. Hatchard, C. A. Parker, A New Sensitive Chemical Actinometer - II. Potassium Ferrioxalate as a Standard Chemical Actinometer. *Proc. R. Soc. London, Ser. A* **235**, 518−536 (1956).

Acknowledgments:

Funding:

National Science Foundation CHE-2243724 (DGN)

National Science Foundation Graduate Research Fellowship Program under Grant DGE-2140743 and the Herchel Smith Graduate Fellowship Program at Harvard University (BMC)

Arnold and Mabel Beckman Foundation for an Arnold O. Beckman Postdoctoral Fellowship (MIG)

National Institute of Health F32GM147975 (JBG)

Advanced Photon Source, an Office of Science User Facility, operated for the U.S. Department of Energy (Office of Science) by Argonne National Laboratory under DOE Contract No. DE-AC02-06CH11357

Author contributions:

Conceptualization: BMC, MN, DGN

Methodology: BMC, JBG, ERR, MIG, KGR

Investigation: BMC, JBG, ERR, MIG, KGR

Funding acquisition: DGN

Writing – original draft: BMC, DGN

Writing – review & editing: BMC, JBG, ERR, MIG, KGR, MN, DGN

Competing interests: Authors declare that they have no competing interests.

Data and materials availability: Metrical data and supplementary crystallographic data for the solid-state structures are available from the Cambridge Crystallographic Data Centre under reference numbers CCDC 2289548-2289554. These data can be obtained free of charge via www.ccdc.cam.ac.uk/data_request/cif, or by emailing data_request@ccdc.cam.ac.uk, or by contacting The Cambridge Crystallographic Data Centre, 12 Union Road, Cambridge CB2 1EZ, UK; fax: +44 1223 336033. All other data are available in the main text or the supplementary materials.

Supplementary materials:

Materials and Methods

Preparation of Compounds

Single Crystal X-ray Structural Characterization

UV-vis-NIR Spectroscopy

Photolysis Experiments

Electrophotocatalysis

Quantum Yield Determination

TRIR Experiments

Figs. S1 to S49

Tables S1 to S3

References (*46–59*)